Superdiffusive Heat Transport in a class of Deterministic One-Dimensional Many-Particle Lorentz gases

Pierre Collet[1], **Jean-Pierre Eckmann**[2,3] **and Carlos Mejía-Monasterio**[4]

[1]Centre de Physique Théorique, CNRS UMR 7644, Ecole Polytechnique, F-91128 Palaiseau Cedex (France)
[2]Département de Physique Théorique, Université de Genève
[3]Section de Mathématiques, Université de Genève
[4]Istituto dei Sistemi Complessi, Consiglio Nazionale delle Ricerche, Sesto Fiorentino Italy

Abstract

We study heat transport in a one-dimensional chain of a finite number N of identical cells, coupled at its boundaries to stochastic particle reservoirs. At the center of each cell, tracer particles collide with fixed scatterers, exchanging momentum. In a recent paper, [1], a spatially continuous version of this model was derived in a scaling regime where the scattering probability of the tracers is $\gamma \sim 1/N$, corresponding to the Grad limit. A Boltzmann-like equation describing the transport of heat was obtained. In this paper, we show numerically that the Boltzmann description obtained in [1] is indeed a bona fide limit of the particle model. Furthermore, we study the heat transport of the model when the scattering probability is 1, corresponding to deterministic dynamics. Thought as a lattice model in which particles jump between different scatterers the motion is persistent, with a persistence probability determined by the mass ratio among particles and scatterers, and a waiting time probability distribution with algebraic tails. We find that the heat and particle currents scale slower than $1/N$, implying that this model exhibits anomalous heat and particle transport.

1 Introduction

The rigorous description of (classical) non-equilibrium steady states (NESS) remains an elusive problem, despite some remarkable progress in the last few years, as described, *e.g.*, in [2, 3, 4]. Indeed, it is usually impossible to guess the stationary state, and this distinguishes non-equilibrium problems from equilibrium problems in statistical mechanics. Therefore, many studies try to find the best descriptions of NESS and aim to understand what the essentials of NESS are and how different models fit together. Among the few works in which some properties of NESS have been obtained, we mention the harmonic chain coupled to Langevin heat baths [5] and anharmonic chains coupled to infinite (non compact) reservoirs [6, 7].

In this paper, we study heat and particle conduction in a 1-dimensional particle model introduced in [1], which is a variant of a model studied in [8, 9]. The model consists of a chain of identical cells, each of which contains a fixed point-like scatterer that exchanges momentum with tracer particles. At its boundaries the chain is in contact with two stochastic particle reservoirs, characterized by a fixed temperature. Inside the system the particles move deterministically between cells, interacting with the scatterers but not among themselves. However, on their passage the particles modify the local state of the substrate, which in turns alters the evolution of the other particles. At the collisions energy and momentum are conserved. For the quasi-1D models of [8, 9], this interaction leads to the establishment of local thermal equilibrium and normal transport. Furthermore, we introduce a coupling strength per cell, given by the probability that, when a particle encounters a scatterer, they exchange momentum. If the chain is composed of N cells, we call this collision probability γ/N, with $\gamma \in [0, N]$. Therefore, the dynamics in the bulk is deterministic only if $\gamma = N$.

Out of equilibrium, *i.e.*, when an open system is subjected to gradients of temperature T and chemical potential μ, steady heat and particle currents (that we call J_Q and J_n respectively), appear. If the gradients are small these currents are linear combinations of the thermodynamic gradients,

$$\mathbf{J} = \mathcal{M}\mathbf{F} \,, \tag{1.1}$$

where $\mathbf{J} = (J_Q, J_n)$, $\mathbf{F} = (\nabla T, \nabla \mu)$ and $\mathcal{M}$ is a 2×2 matrix that is symmetric by virtue of the Onsager's reciprocity theorem. For instance, if $J_n = 0$ then (1.1) yields the well known Fourier's law relating the heat flux with the temperature gradient. Moreover, (1.1) implies that, if the conductivities in $\mathcal{M}$ do not depend explicitly on the size N of the system then the currents scale as $\mathbf{J} \sim 1/N$. In the

literature, it is customary to call this scaling *normal* transport as, combined with the conservation laws, (1.1) implies that the densities are diffusive fields.

We analyze the equilibrium and nonequilibrium transport properties of the particle model with a finite number N of cells and focus on two variants: a stochastic model with $\gamma = 1$ and the deterministic model. We show numerically that in the limit of large N, the Boltzmann description of the model obtained in [1] is a bona fide limit of the stochastic particle model. Furthermore, we find that neither the stochastic nor the deterministic models satisfy the Fourier's law: in the stochastic model the transport is ballistic, *i.e.*, the currents scale as $\mathbf{J} \sim N$. Instead, the deterministic model exhibits superdiffusive transport with the currents scaling as $\mathbf{J} \approx N^{-0.4\pm0.02}$.

In the next section we describe in detail the model and in Sect. 3 we discuss the general properties of its non-equilibrium steady state. In Sect. 4 we study the continuous limit of the stochastic model and compare it with the theory that appeared in [1]. Finally, in Sects. 5 and 6 we discuss the energy and particle transport of the finite deterministic chain.

2 The Model

In this section, we describe the 1-dimensional particle model that we consider, and briefly review the results of [1] for the continuous model.

The model consists of N cells in a row, each cell of length λ. In the center of each cell there is a point-like scatterer which does not move but which has a "momentum" $P \in \mathbb{R}$ and a mass M. Particles move in these cells. They have mass $m \neq M$ and momentum p. The particles do not interact among themselves but they do interact with the scatterers as follows: Whenever a particle with momentum p reaches a scatterer whose momentum is P, the following happens: With probability $1 - \gamma/N$, the particle crosses to the other side of the scatterer, and continues with momentum p, while the scatterer retains its momentum P. With probability γ/N actual scattering takes place and the new momenta $\tilde{p}$ and $\tilde{P}$ are given by

$$\begin{pmatrix} \tilde{p} \\ \tilde{P} \end{pmatrix} = S \begin{pmatrix} p \\ P \end{pmatrix} ,$$

where the scattering matrix S is

$$S = \begin{pmatrix} -\sigma & 1-\sigma \\ 1+\sigma & \sigma \end{pmatrix} , \quad \text{and} \quad \sigma = (M-m)/(M+m) . \tag{2.1}$$

When $\gamma = N$, the particles interact with the scatterer every time they encounter one and, except for the nature of the baths, the dynamics is fully deterministic. These rules are similar in spirit (but far more rich), to the flipping Lorentz lattice gases studied some years ago [10]. When $\gamma < N$ the model has some randomness, since for each encounter of a particle with a scatterer, we need to decide if scattering takes place, or if the particle traverses the scatterer.

The collision rules (2.1) are just those of elastic scattering, but with the scatterers not moving. The deterministic model (with $\gamma = N$) is a one dimensional generalization of the quasi-one dimensional models previously studied in [8, 9, 11, 12], where the scatterers are fixed, freely rotating disks. In these models, the collisions provide a local energy mixing among different degrees of freedom that leads to a local state which is well approximated by a local equilibrium state, where the particles behave as a perfect gas. Close to equilibrium, Green-Kubo relations for the heat and particle fluxes are valid and the corresponding Onsager reciprocity relations are satisfied [8, 11]. Moreover, in the zero-coupling limit, where the invariant measure of the NESS is expected to be a multivariate Gaussian, compact analytical expressions for the currents and the density profiles have been obtained [9]. To the lowest order, the corrections due to a finite coupling were considered in [12]. In [13], the same collision rules with $\gamma = N$, have been considered to study the trajectories of one single particle.

In the bulk, the dynamics preserves the total energy and total momentum in the system irrespective of the values of σ and γ. Note that the total energy and total momentum of the particles is not a conserved quantity, since arbitrary amounts of energy and momentum can be stored by the set of scatterers. Only if $\sigma = 0$ *i.e.*, if particles and scatterers have the same mass the energies and momenta of the particles are "weakly" conserved, in the sense that the particles exchange the initial value of their momenta among themselves through different collisions with the scatterers.

To force the system out of equilibrium, we couple the leftmost and rightmost cells to infinite ideal particle reservoirs. These reservoirs are not a perfect gas at temperature T, but should rather be viewed as an infinite bulk of particles and scatterers of our model at equilibrium temperature T. From each reservoir particles are injected into the system at a given rate ν and with momenta distributed according to

$$F^{\pm}(p)\, dp \;=\; \Theta(\pm p)\, (2\pi m k_{\rm B} T)^{-1/2}\, e^{-p^2/2mk_{\rm B}T}\, dp\,, \tag{2.2}$$

where T is the temperature of the reservoir, $k_{\rm B}$ the Boltzmann constant and the Heaviside function $\Theta(p)$ restricts the sign of the momentum according to the side

from where the particles are injected ("$-$" for those entering from the right side and "$+$" for those entering from the left). Equation (2.2) implies that the momentum distribution $f(p)$ of the particles inside any given cell, have a momentum density $f(p)$ with a non-normalizable singularity at $p = 0$. This also applies for the particle momentum distribution of the reservoirs. For the reservoir coupled to the leftmost ($i = 1$) cell, $f(p)$ is

$$f_{\rm L}(p)\,dp \;=\; \frac{\Theta(+p)}{(2\pi m k_{\rm B} T_{\rm L})^{1/2}} \frac{e^{-p^2/2mk_{\rm B}T_{\rm L}}}{|p|}\,dp\,, \tag{2.3}$$

and for the reservoir coupled to the rightmost ($i = N$) cell

$$f_{\rm R}(p)\,dp \;=\; \frac{\Theta(-p)}{(2\pi m k_{\rm B} T_{\rm R})^{1/2}} \frac{e^{-p^2/2mk_{\rm B}T_{\rm R}}}{|p|}\,dp\,. \tag{2.4}$$

The distribution of the injected particles (2.2) is chosen so that the momentum distribution of the scatterers, are Maxwellian in equilibrium ***i.e.***, when both reservoirs are at the same temperature $T_{\rm L} = T_{\rm R}$. More precisely, denoting by $g_i(P)$ the distribution of the momentum of the i-th scatterer and by $F_i(p) = |p| f_i(p)$, where $f_i(p)$ is the momentum distribution of the particles in the i-th cell, in [1] it has been shown that if the particle injection rates are the same ($\nu_{\rm L} = \nu_{\rm R}$) and $T_{\rm L} = T_{\rm R} = T$, then F and g are both Gaussian and are given by

$$F(p)\,dp \;=\; (2\pi m k_{\rm B} T)^{-1/2} e^{-p^2/2mk_{\rm B}T}\,dp\,, \tag{2.5}$$

$$g(P)\,dP \;=\; (2\pi M k_{\rm B} T)^{-1/2}\, e^{-P^2/2Mk_{\rm B}T}\,dP\,, \tag{2.6}$$

irrespective of i. Here, we illustrate this numerically. We have considered a chain of $N = 30$ cells with $\gamma = N$ in equilibrium. The masses were chosen $m = 1$[1] and $M = 3$, so that $\sigma = 0.5$. In Fig. 1-a, the distributions $g_i(P)$ (dashed) and $F_i(p)$ (solid) are shown. Both coincide with the respective Maxwellian distribution (not shown), at a temperature T equal to the equilibrium temperature fixed by the reservoirs. Moreover, the same distributions are found irrespective of the cell i in which they are sampled.

If particles do not interact, then the momentum distribution of the injected particles that preserves the equilibrium state becomes $|p|F^{\pm}(p)dp$ (see ***e.g.*** [14]). Indeed, the infinite invariant measure $f(p)$ is a consequence of the particular dynamics of our system. The singularity of $f(p)$ is non-integrable only for models

[1] In what follows, we fix the particle mass to 1.

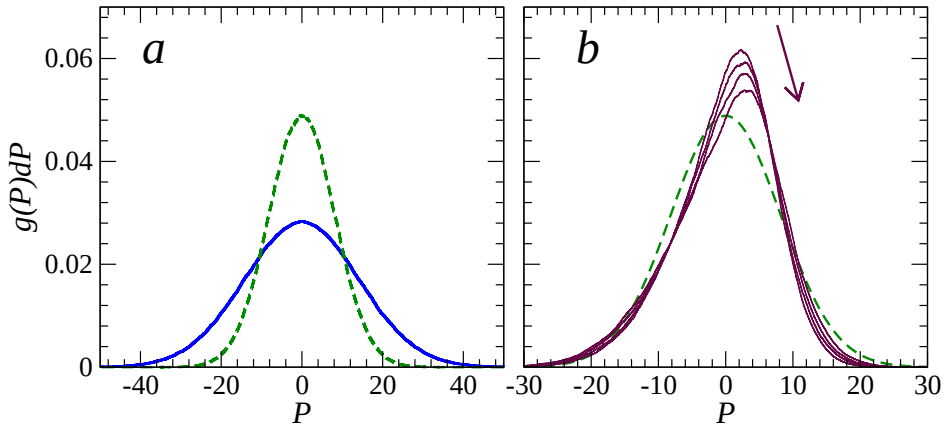

Figure 1: Momentum distribution of particles and scatterers for a chain of $N = 30$ cells, $\sigma = 0.5$ at equilibrium (panel *a*) and out of equilibrium (panel *b*). In panel *a* the momentum distributions $g_i(P)$ (dashed curve) and $F_i(p)$ are plotted for $\nu_{\rm L} = \nu_{\rm R} = 240$, $T_{\rm L} = T_{\rm R} = 200$. They coincide with the equilibrium distributions at the temperature of the reservoirs. Moreover, they do not depend on the cell i in which they are sampled. In panel *b* (see section 3), we show the scatterer's momentum distribution $g_i(P)$ for $i = 1$, 10, 20 and 30 (in the order indicated by the arrow), with $\nu_{\rm L} = 240$, $\nu_{\rm R} = 140$, $T_{\rm L} = 100$ and $T_{\rm R} = 300$. As a reference, the equilibrium distribution $g(P)$ of panel *a* is also plotted (dashed curve).

with one dimensional dynamics. [2] This is related to the fact that, while in any dimension slow particles need much longer times to move across the system than fast particles, only in 1-dimensional dynamics this imply that particles steadily accumulate near $p = 0$.

Another consequence of the infinite invariant measure $f(p)dp$ is that in the stationary state (the time $t \to \infty$), the number of particles in the system is infinite. Starting with any initial distribution, and letting the system evolve in time t, the number of particles with low momenta grows without bounds. On the other hand if one can prove that the number of particles with momentum $p > p_0$ has a limit as $t \to \infty$ then the stationary state is well defined, in spite of the divergence of the total number of particles. To illustrate this, we have measured the evolution in time of the number of particles in the system and their momentum distribution, for a chain of $N = 201$ cells in equilibrium, with $\nu_{\rm L} = \nu_{\rm R} = 100$ and $T_{\rm L} = T_{\rm R} =$

[2] In higher dimensions, $1/|p|$ is integrable near $p = 0$.

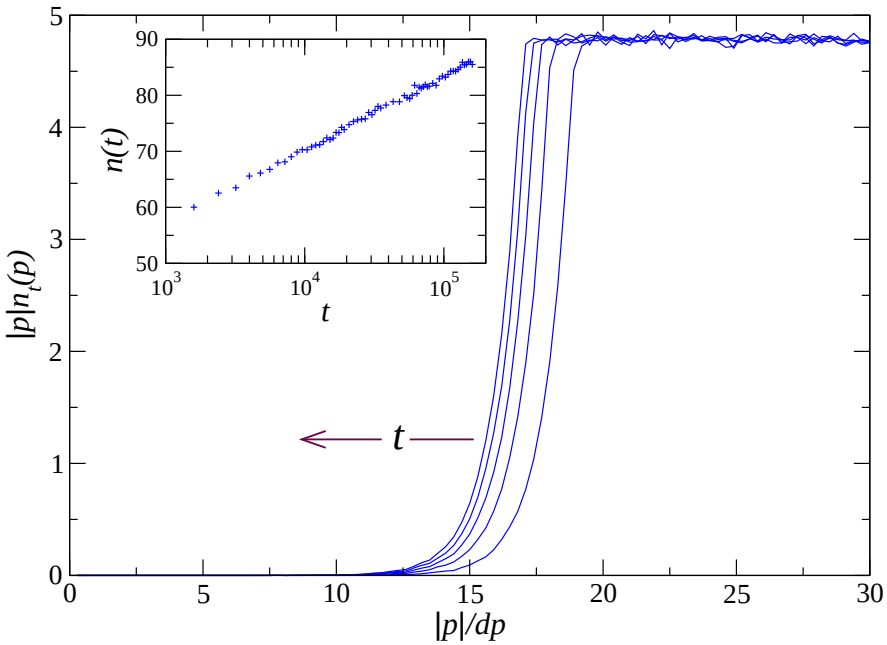

Figure 2: Number of particles $n_t(p)$ with momentum $\approx p$ times the momentum $|p|$, at $t = 200$, 600, 1000, 1400 and 1800, for a chain of $N = 201$ cells at equilibrium with $\nu_{\mathrm{L}} = \nu_{\mathrm{R}} = 100$ and $T_{\mathrm{L}} = T_{\mathrm{R}} = 100$, $\sigma = 1/2$ and $\gamma = N$. dp is the width of the bins used to compute the empirical distribution $n_t(p)$. Thus, the x-axis corresponds to the bin number. In the inset: logarithmic divergence of the total number of particles inside the system.

100. We find that the number of particles inside the system, defined as $n(t) = \int_{-\infty}^{\infty} n_t(p)\, dp$, diverges logarithmically in time, due to the slow accumulation of cold particles (inset of Fig. 2). In Fig. 2, $|p|n_t(p)$ is shown for several successive times. We observe that for p larger than some $p_0(t)$, $|p|n_t(p)$ is invariant. Naturally, the divergence of $n_t(p)$ is limited to the set of very slow particles. Therefore, the singularity of $f(p)$ does not affect the properties of transport, as small velocity particles do not contribute to it.[3] Similar conclusions have been obtained in other contexts in [15, 16].

We conclude this section by briefly reviewing the continuum limit studied in [1]. In the limit of $N \to \infty$, setting $x = i/(N \cdot \lambda)$ for the position of the i-th

[3] In the same vein, $p_0(t)$ is seen to decrease to zero logarithmically.

cell, $g(P_i) \to g(P, x)$, is the probability density that the scatterer at position x has momentum P and so $\int dP\, g(P, x) = 1$, by definition. In [1] it was argued that in the continuous limit, this system can be modeled by a Boltzmann equation, whose stationary solution is described by the equations

$$p\partial_x F(p, x) = \gamma|p| \int dP \, \Big(F(\tilde{p}, x) g(\tilde{P}\,, x) - F(p, x) g(P\,, x) \Big) \;, \quad \text{(2.7a)}$$

$$0 = \int dp \, \Big(F(\tilde{p}, x) g(\tilde{P}\,, x) - F(p, x) g(P\,, x) \Big) \;, \quad \text{(2.7b)}$$

where the quantity $F(p, x)$ is equal to $F(p, x) = |p| f(p, x)$, with $f(p, x)$ the probability density that a particle at position x has momentum p, and $\gamma \in [0, N]$ corresponds to the same quantity of the particle model, which determines the scattering probability. Therefore, for $p > 0$, $F(p, x)$ is related to the rate of particles with momentum p moving from x to the right. Similarly, $F(p, x)$ is, for $p < 0$, related to the rate of particles with momentum p moving from x to the left. Note that, in contrast to $f(p)$, the function $F(p)$ is free of singularities. Therefore, in spite of the infinite number of particles in the stationary state of the scattering model, the flux $F(p, x)$ is finite and integrable, and it is for this quantity that the Boltzmann equation is formulated.

The Boltzmann equation (2.7) was derived assuming that $F(p)$ and $g(P)$ are statistically independent. Therefore, the similarity between the particle model and its Boltzmann version should be best in the case of large N and when there are many particles (with momentum $|p| > p_0 > 0$) in each cell. Moreover, in [1], it was proven that for any particle injections $f_{\mathrm{L}}(p)$ and $f_{\mathrm{R}}(p)$ in a certain cone in Banach space, (2.7) has solutions when $\gamma = \mathcal{O}(1)$. Our numerical studies are, however, for parameter values well outside this cone, and still give a very good comparison between the particle model and the Boltzmann model. Furthermore, when $\gamma = \mathcal{O}(N)$, the particle model is still well defined, although different from the Boltzmann model. If $\gamma = N$ a particle will scatter whenever it meets a scatterer and will never fly to the other side of a scatterer without collision. When $\gamma \ll N$, the local state cannot correspond to a local equilibrium state. Indeed, when scattering is rare, the particles do not interact, thus leading to local states that are described by the sum of two different families of particles: those that were injected from the left, flying ballistically to the right, and those injected from the right that fly ballistically to the left [17]. However, if $\gamma = N$, then all particles scatter when they encounter a scatterer, leading to a stronger local interaction. One would expect that this strong interaction would lead to a diffusive

particle behavior. However, in Sect. 5, we will show that the transport remains superdiffusive.

3 Non-equilibrium steady state

In this section we study the nonequilibrium properties of our model. Here and in what follows, we will limit ourselves to study the stochastic model given by $\gamma = 1$ and the deterministic one corresponding to $\gamma = N$. This stochastic model corresponds to the Grad limit considered in [1].

We start by defining the particle and energy injection rates. The particle injection rates from the left and right reservoirs (denoted by $\nu_{\rm L}$ and $\nu_{\rm R}$ respectively) are defined is terms of the momentum distribution of the injected particles (2.2) as

$$\nu_{\rm L} = \int_0^\infty F^+(p)dp \quad \text{and} \quad \nu_{\rm R} = \int_\infty^0 F^-(p)dp \,. \tag{3.1}$$

As we have discussed, the particle density in the bath is infinite. However, since the integral in (3.1) is finite, one realizes that ν takes the role of an effective particle density. The rate at which energy is injected into the system from each reservoir are determined by the particle injection rates simply as

$$\varepsilon_{\rm L/R} = \nu_{\rm L/R}\, k_{\rm B} T_{\rm L/R} \,. \tag{3.2}$$

Setting ν and ε of both reservoirs, fixes the nonequilibrium state. Moreover, local differences of these rates determine the currents. If the state fixed by the reservoirs' rates is very far from equilibrium then the identification of a local temperature in the bulk of the system becomes problematic as the momentum distributions $F(p)$ and $g(P)$ have large deviations from Gaussian. We illustrate this in the Fig. 1-b where $g_i(P)$ is shown for $i = 1$ being the leftmost cell, 10, 20 and 30 being the rightmost cell. Naturally, as the scatterers feel the nonequilibrium state set at the boundaries, $g_i(P)$ is not longer uniform with respect to the position i. Furthermore, for all i, $g_i(P)$ is far from being an equilibrium distribution.[4] The particle momentum distribution $F(p)$ will be discussed in section 4.

In Fig. 3 we compare the particle density $\varrho(x)$ and the temperature profiles numerically obtained for the stochastic ($\gamma = 1$) and the deterministic models. The temperature at the i-th cell is computed as $\langle p^2 \rangle$ averaged with respect to the

[4] In what follows, we shall take care of studying nonequilibrium states, for which the local temperature or at least, a good approximation of it, can be determined.

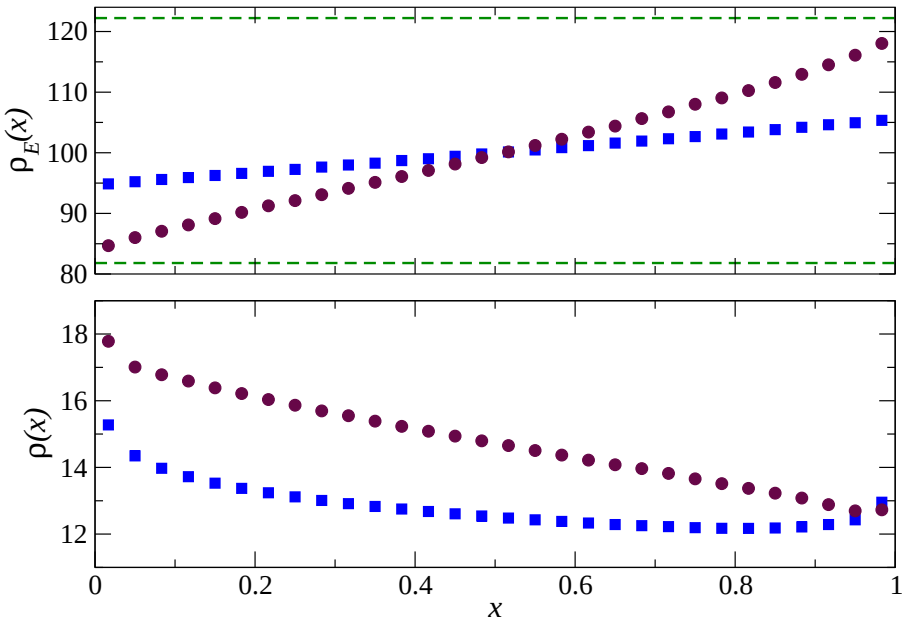

Figure 3: Profiles of the particle density (lower panel) and the kinetic energy per particle density E_K (upper panel), for a chain of $N = 30$ cells, $\sigma = 0.5$ and for $\gamma = 1$ (squares), and $\gamma = N$ (circles). Particles were injected to the chain with rates $\nu_{\rm L} = 220$, $\nu_{\rm R} = 180$ and temperatures $T_{\rm L} = 81.818$ and $T_{\rm R} = 122.222$, indicated here by the dashed line.

particle momentum distribution function $F_i(p)$ measured at the i-th cell. This temperature coincides with the time averaged kinetic energy of the i-th scatterer, indicating a good local equilibration. All the observables were averaged for a time interval during which the total number of particles inside the channel does not change appreciably.

As commonly observed, the temperature in the bulk of the system of both models does not match the nominal temperatures of the reservoirs (indicated by the dashed lines in the upper panel). Moreover, the energy mismatch at the contacts with the reservoirs depends on the scattering probability. This is natural as γ is proportional to the effective bulk resistance of the system. This means that, lower values of γ translate into larger nonequilibrium currents. Therefore, since the energy jumps at the contacts must be proportional to the energy current, they are larger for the stochastic model than for the deterministic one. In the bulk of

the system, the temperature profile for $\gamma = 1$ is less steep than for $\gamma = N$ since in the former case, particle-particle interaction, mediated by the scatterers, is less effective than in the latter case. As for the particle density, a smaller scattering probability leads to a less steep density profile. Moreover, the accumulation of particles at the contact with the reservoirs is more pronounced when the scattering is less frequent. This is because the scattering contributes to heat up the injected cold particles.

Out of equilibrium, the particles inside the cell at position x, leave the cell to the right at a different rate than the rate at which they leave the cell to the left. This is a consequence of the substrate-mediated particle-particle interaction. Calling the rate at which particles cross from one cell to another from left to right $\nu_{\mathrm{R}}(x)$ and from right to left $\nu_{\mathrm{L}}(x)$, the particle current is defined as

$$J_n(x) = \nu_{\mathrm{R}}(x) - \nu_{\mathrm{L}}(x + dx) \, . \tag{3.3}$$

Therefore, these local rates are strongly dynamically constrained, so that the stationary particle current is uniform. Indeed, we find that, in the stationary state, a uniform particle current, with extremely linear profiles for $\nu_{\mathrm{R}}(x)$ and $\nu_{\mathrm{L}}(x)$. In Sect. 5, we will see that these strong correlations determine an unexpected superdiffusive particle and energy transport.

4 Infinite volume limit: $\gamma = 1$

In this section, we compare the non-equilibrium probability distribution functions of the discrete model with those predicted by the Boltzmann equation (2.7).

We have solved numerically (2.7) by a discretization in momentum space. Fixing the spacing of the discretized momentum to Δp, the number of points we considered is the minimum necessary to keep the information from the tails of the distributions as small as $\sim 10^{-10}$. We proceed as follows: at any x, the equation (2.7b) for g only depends on $F(\cdot, x)$. We discretize (2.7b) and solve it as an eigenvalue problem (with eigenvector $g(\cdot, x)$). The only limitation is the size of the matrices one obtains in this way: Our runs were done with matrices of size ~ 4200. The function g found in this way is then inserted into (2.7a). High-order integration in position space is then used to integrate (2.7a) from $x = 0$ to $x = 1$. Therefore, fixing the injection at $x = 0$ to (2.3), we use a shooting method to determine the extraction of particles at $x = 0$ in such a way that at $x = 1$ the desired injection (2.4) will result (see also [1] for more details).

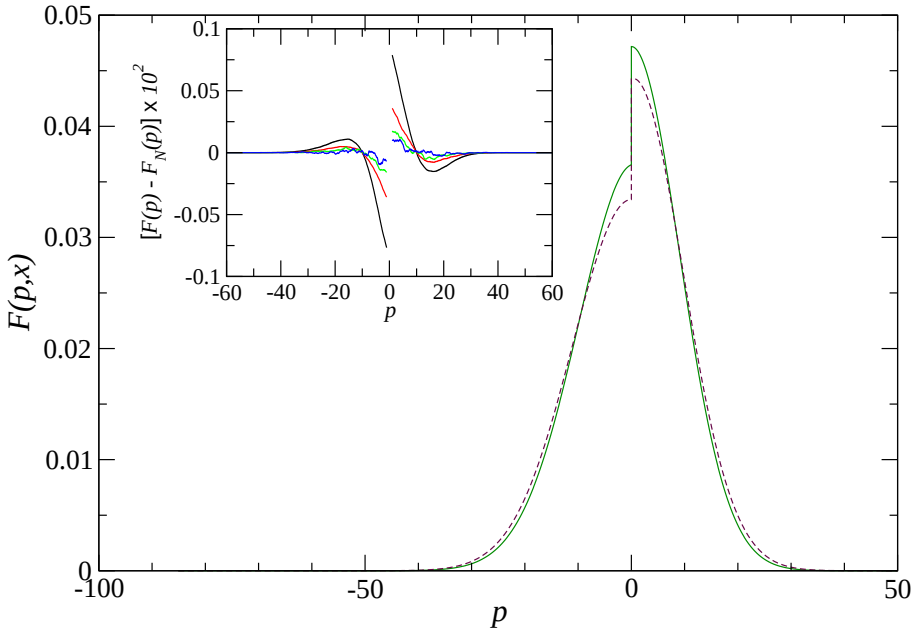

Figure 4: Momentum distribution $F(p, x)$ of the particles at the left (solid curve) and right (dashed curve) ends of the system , from the solution of the Boltzmann equation (2.7), for $\sigma = 0.5$, $\nu_{\rm L} = 220$, $\nu_{\rm R} = 180$, $T_{\rm L} = 81.818$ and $T_{\rm R} = 122.222$. In the inset the finite size deviation of $F_N(p, x)$ from the Boltzmann solution are shown for $N = 2$ (black), $N = 4$ (red), $N = 8$ (green) and $N = 16$ (blue).

In Fig. 4 we show the solution of (2.7) for $\sigma = 0.5$, $\nu_{\rm L} = 220$, $\nu_{\rm R} = 180$, $T_{\rm L} = 81.818$ and $T_{\rm R} = 122.222$, and $\gamma = 1$. The first peculiarity of the non-equilibrium distributions is the jump at $p = 0$. This is due to the very weak particle-particle interaction obtained for $\gamma = 1$. The size of the jump is partly determined by γ and, as it is clear from Eq. (3.1), partly by the difference between $\nu_{\rm L}$ and $\nu_{\rm R}$. Note that, as a consequence of the temperature gradient, the positive and negative parts of the distribution are only approximately Gaussian. They are Gaussian only if $T_{\rm L} = T_{\rm R}$.

To study the limit $N \to \infty$, we have numerically followed the evolution of finite size N chains and measured the particle momentum distribution $F_N(p, x)$ for the same parameters as above. In the inset of Fig. 4, the deviation of $F_N(p, x)$ from the solution of the Boltzmann equation $F(p, x)$ is shown for chains from $N = 2$ to $N = 16$.

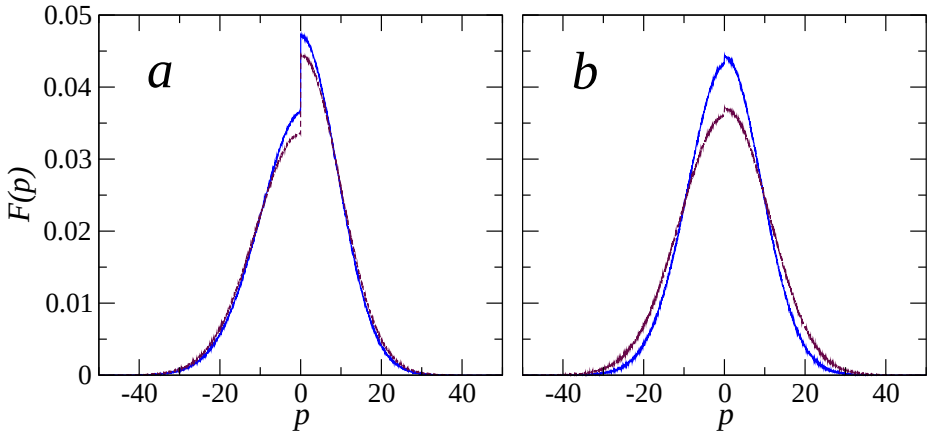

Figure 5: Momentum distribution $F_N(p,x)$ of the particles at $x = 1/N$ (solid curve) and $x = 1$ (dashed curve), for a chain of $N = 30$ cells, with $\sigma = 0.5$, for a) $\gamma = 1$ and b) $\gamma = N$. The bath's parameters are as in Fig. 4.

Deviations are seen over the whole domain, although they are biggest at the center of the distribution. They are not symmetric in p, which is an indication that, for a given size N, deviations may depend on the injection rates and bath's temperatures in general. Furthermore, we observe that the solution of (2.7) appears to be the asymptotic distribution, $\lim_{N\to\infty} F_N(p,x) \to F(p,x)$. In any case, the deviations from $F(p,x)$ are less than 0.1%, tending to zero very fast. For instance, for a chain of $N = 16$ the deviations are less than 0.01%.

Finally, we have also measured the distribution $F_N(p,x)$ for the deterministic finite chain ($\gamma = N$). In Fig. 5, we show $F_N(p,x)$ at $x = 1/N$ (solid curve) and $x = 1$ (dashed curve), for a chain of $N = 30$ cells and $\gamma = 1$ (panel a), $\gamma = N$ (panel b). The other parameters are reported in the caption of Fig. 4. The distributions $F_{30}(p,x)$ in Fig. 5-a, are on top of the solution (2.7) and, as mentioned above, the deviations from the asymptotic distribution decay very fast. For $\gamma = N$, the jump at $p = 0$ is much smaller, with the only remaining contribution coming from the difference $|\nu_{\rm L} - \nu_{\rm R}|$ of the injection rates. For both models, $F(p)$ is not Gaussian, even if $\nu_{\rm L} = \nu_{\rm R}$ (not shown).

5 Energy transport

In this section we turn our attention to the heat transport of the deterministic model, *i.e.*, setting $\gamma = N$. The particles of mass m are the only energy carriers of the system. We start by analyzing their dynamics.

5.1 Microscopic evolution

We consider a finite chain of N cells with periodic boundary conditions and n particles *per cell*. A stationary state of this closed system is the equilibrium state characterized by N, n and the total energy E given by

$$E_0 = \frac{1}{2}\left(\frac{1}{m}\sum_{i=1}^{nN} p_i^2 + \frac{1}{M}\sum_{i=1}^{N} P_i^2\right) . \tag{5.1}$$

We start the evolution with the scatterers at 0 momenta. As for the open chain, the state of the system approaches equilibrium logarithmically slowly (in time). During the transient, the substrate continuously extracts energy from the gas of particles; the total energy of the scatterers grows logarithmically in time, until it saturates at sufficiently long times. All measurements are taken after the system has relaxed to the approximate equilibrium state.

Once equilibrium is reached, we follow the evolution of a tagged particle, for N and n sufficiently large.[5] Here, we are interested in the high density regime, which, following the discussion about Fig. 2, is a good approximation of the stationary $n = \infty$ state.

When the particle encounters a scatterer, its velocity after the collision is determined by (2.1). In fact, this scattering matrix leads to a persistent motion of the particle, namely the probability that the particle continues in the same direction in which it reached the scatterer, is larger than $1/2$. This probability, μ, can be easily computed as follows[6]: without loss of generality assume that before the collision, the particle's velocity is $v > 0$. In equilibrium, the scatterer velocity distribution function is obtained by taking $V = P/M$ in (2.6). Taking into account that after the collision the particle's velocity is $v' = -\sigma v + (1+\sigma)V$ (see (2.1)), the probability that after the collision the particle has a velocity $v' > 0$ can be written

[5] Since particles interact among themselves only through their collisions with the substrate, the local dynamics may depend on the finite time particle density.

[6] To analyze the dependence of μ on the masses, it is convenient to work with the velocities instead of the momenta.

as[7]

$$\mu(\sigma) \equiv P(v' > 0 | v > 0) = \frac{(mM)^{1/2}}{2\pi k_{\rm B} T} \int_0^\infty dv \; e^{-\frac{mv^2}{2k_{\rm B}T}} \int_{\frac{\sigma}{1+\sigma}v}^\infty dV e^{-\frac{MV^2}{2k_{\rm B}T}} \; , \quad (5.2)$$

that can be integrated to yield

$$\mu(\sigma) = \frac{1}{2} - \left(\frac{m}{2\pi k_{\rm B} T} \right)^{1/2} \int_0^\infty dv \; \mathrm{erf} \left(\frac{(M-m)v}{(8Mk_{\rm B}T)^{1/2}} \right) e^{-\frac{mv^2}{2k_{\rm B}T}} \; , \quad (5.3)$$

where erf$(\cdot)$ is the error function. The limit values of μ can be easily read from (5.3): for $\sigma = -1$, namely $M = 0$, the error function is erf$(-\infty) = -1$ and $\mu = 1$. In the opposite case, when $\sigma = 1$ ($M = \infty$), $\mu = 0$. Finally, for $\sigma = 0$, namely $M = m$, erf$(0) = 0$ and $\mu = 1/2$. With the exception of $\sigma = 0$, the dynamics of the particles is persistent. In Fig. 6, the probability $\mu(\sigma)$, computed from the statistics of the collisions of the tagged particle is shown.

Neglecting the interaction between particles, we can simplify the model, studying the dynamics on the lattice. If we do so, then the particle can be seen as a persistent random walk that hopes from scatterer to scatterer with a waiting time τ that corresponds to the collision times *i.e.*, proportional to the inverse of the particle's velocity after the last collision.

We have measured the distribution of the waiting time $\Psi(\tau)$ of the tagged particle for different values of σ. In Fig. 7 we show $\Psi(\tau)$ for $\sigma = 0$ and $\sigma = 0.5$. As a consequence of the single particle's velocity distribution, $\Psi(\tau)$ turns out to be a broad distribution $\Psi(\tau) \simeq \tau^{-(1+s)}$. Our persistent walker seemingly performs a Levy walk. From a fit to a power law of the numerical distributions $\Psi(\tau)$ we obtain that for $\sigma = 0.5$, $s = 0.99 \pm 0.02$ and for $\sigma = 0$, $s = 2.07 \pm 0.07$. For different values of σ (not shown), we find that $s \approx 1$.[8] We cast these results as

$$\Psi(\tau) \sim \begin{cases} \tau^{-3} & \text{for} \quad \sigma = 0 \\ \tau^{-2} & \text{for} \quad \sigma \neq 0 \end{cases} \; . \quad (5.4)$$

In the continuous limit, a persistent random walker yields to a particle's density whose evolution is described by the telegrapher's equation [18]. Noting that asymptotically the telegrapher's equation yields to a diffusive evolution and that the Levy walk for $1 < s < 2$ does only induce anomalous corrections to the

[7] There is no factor $1/|v|$ here, because we must consider the probability of a particle with velocity in $[v, v + dv]$ hitting a scatterer within a given time.

[8] The power -2 for $\sigma \neq 0$ can be derived (approximately) from a multiple integral as in (5.3).

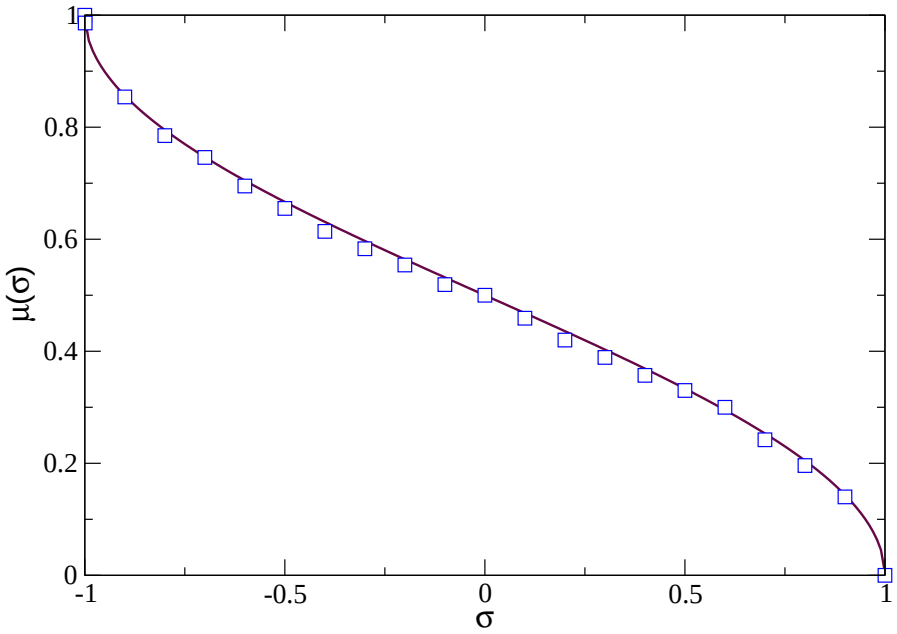

Figure 6: Persistent probability μ as a function of the mass ratio parameter σ, averaged over the evolution of a tagged particle in a chain of $N = 11$, $n = 20$ and $T = 500$. The solid curve corresponds to Eq.(5.3).

normal long-time behavior [19], one would expect that the microscopic particle's dynamics yields diffusive transport. However, this is not the case. In Fig. 8 we show the evolution of the dispersion of the position of a tagged particle $\langle x^2(t)\rangle$ for $\sigma = 0.5$, averaged over an ensemble of initial conditions. Asymptotically, $\langle x^2(t)\rangle \sim t^\alpha$, with $\alpha \lesssim 2$. In fact, we have found that the asymptotic scaling of $\langle x^2(t)\rangle$ depends on the mass ratio parameter σ (see inset of Fig. 8). Being the scaling an asymptotic property that we measure at large but finite times, we cannot discard the possibility that, measured at later times, $\alpha(\sigma)$ will gets closer to 2, indicating that the particle transport is always ballistic. Here, we limit ourselves to report our findings. Therefore, for $\sigma = 0$ the particle's motion seems to be ballistic, while for $\sigma \neq 0$, the motion seems to be superdiffusive. The observed anomalous behavior proves that in one dimension, the effect of the dynamical memory of the deterministic model is much stronger than in higher dimensions[9].

[9]Note incidentally that, if the direction of the particle after the collision if chosen randomly so that the effects of the dynamical memory can be neglected, then diffusive transport is recovered.

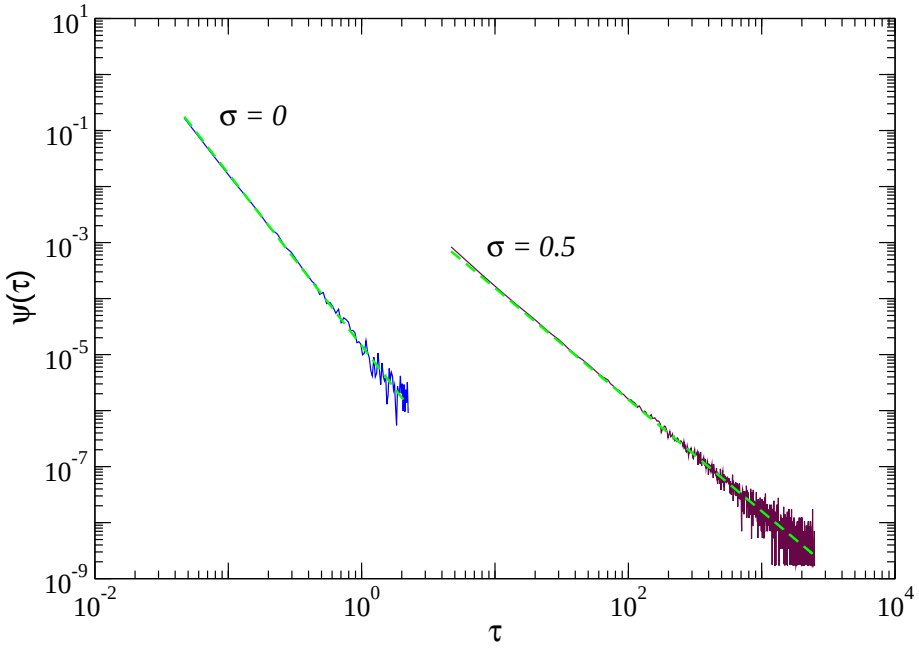

Figure 7: Distribution function of the collision times $\Psi(\tau)$, for $\sigma = 0$ and $\sigma = 0.5$. The dashed lines correspond to power law fits, namely $\Psi(\tau) \sim \tau^{-3.07\pm0.09}$ for $\sigma = 0$ and $\Psi(\tau) \sim \tau^{-1.99\pm0.02}$ for $\sigma = 0.5$.

Since the particles are the energy carriers one expects that the energy transport will be anomalous as well. We study this in the next section.

6 Heat conductivity

We turn our attention to the energy transport of our model. Considering the open system coupled at its boundaries to two particle reservoirs, we have computed the dependence of the heat conductivity κ on the size of the system N, for fixed nominal values of the injections and temperatures of the particle reservoirs. We define the heat conductivity as

$$\kappa = \frac{N J_U}{T_N - T_1} \,, \tag{6.1}$$

where J_U is the measured energy current and T_1 (resp. T_N) is the temperature measured in the leftmost (resp. rightmost) cell that, as we have seen, in general does

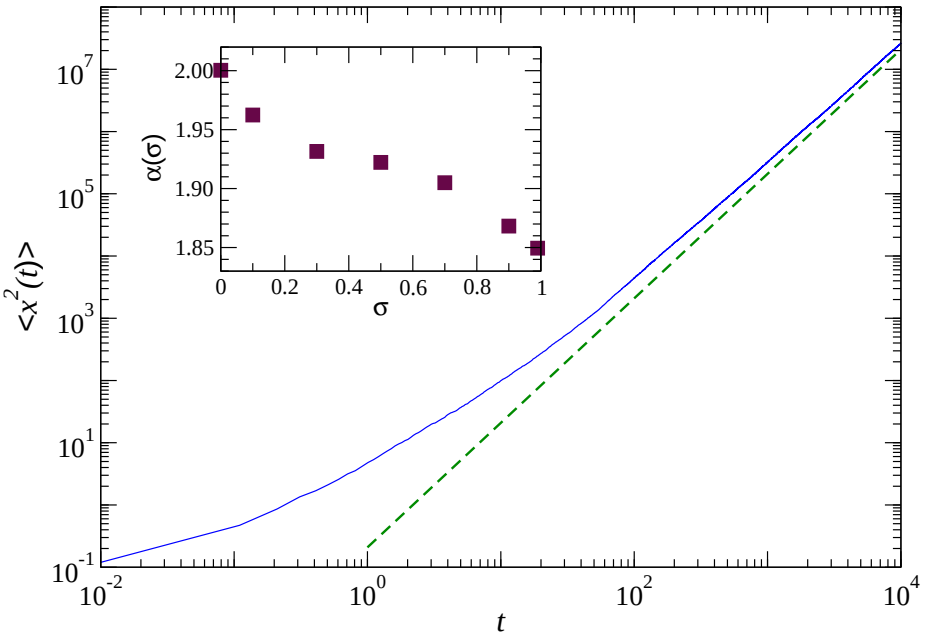

Figure 8: Time dependence of the variance of the position of the tagged particle $\langle x^2(t)\rangle$ averaged over an ensemble of $\mathcal{O}(10^3)$ trajectories, for $N = 11$, $n = 20$ and temperature $T = 500$ (solid curve), when $\sigma = 1$. The dashed line corresponds to a scaling $\sim t^2$. In the inset, asymptotic power scaling $\langle x^2(t)\rangle \sim t^\alpha$, as a function of the mass ratio parameter σ.

not coincide with the temperatures of the reservoirs.[10] Moreover, the temperature difference slightly depends on N.

In our simulations, the currents are measured at a finite time t, when the particle's density $n(t)$ is also finite. Therefore, to study the scaling of J_U and thus of κ, it is important to compute κ from (6.1) at constant $n(t)$. The length of the system is 1 since we space the scatterers by $\lambda = 1/N$. The results of simulations are shown in Fig. 9 for $\gamma = 1$ (circles) and $\gamma = N$ (squares). For the stochastic model ($\gamma = 1$), we obtain $\kappa \sim N$. Particles move ballistically, simply because they interact with the substrate very rarely.[11]

[10] We have found that the temperature profile is, in good approximation, linear when the product of the injection rates $\nu\epsilon = \nu^2 T$ is the same at both boundaries.

[11] The number of times that a typical particle collides with a scatterer before being re-absorbed is $\mathcal{O}(1)$.

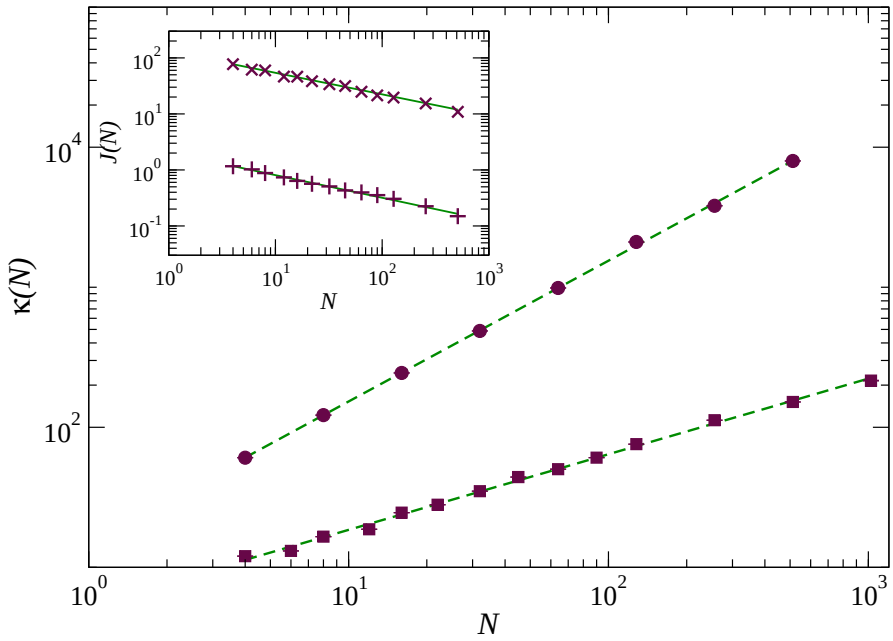

Figure 9: Heat conductivity κ, as a function of the number of cells N, for $\sigma = 0.5$ and $\gamma = N$ (squares) and $\gamma = 1$ (circles). The *reservoirs* were set to $\nu_{\mathrm{L}} = 220$, $\nu_{\mathrm{R}} = 180$, $T_{\mathrm{L}} = 81.818$ and $T_{\mathrm{R}} = 122.222$. The dashed lines correspond to linear fits from which we obtain that for the deterministic model that κ diverges as $\sim N^{0.54\pm0.03}$ and for the stochastic model ($\gamma = 1$), $\kappa \sim N^{1.00\pm0.02}$. These power laws are indicated by the dashed lines. Inset: scaling with N of the energy (cross) and particle (plus) currents of the deterministic model. From fit to power law (solid lines), we obtain that $J_U \sim N^{-0.39\pm0.03}$ and $J_n \sim N^{-0.4\pm0.02}$.

Surprisingly, the transport of the deterministic model is anomalous. First, in the inset of Fig. 9 the scaling with N of the energy and particle currents is shown. Within numerical accuracy, both scale as $\approx N^{-2/5}$. From the conservation of energy it follows that the heat current is $J_Q = J_U - \mu J_n$, where μ is the value of the chemical potential in the bulk. Therefore, using this and the fact that J_U and J_n scale with the same power law, we conclude that $J_Q \approx N^{-2/5}$ as well. More importantly, the scaling of κ as defined in (6.1) coincides with the scaling of the *real* thermal conductivity. We find that the thermal conductivity diverges as $\kappa \sim N^{0.54\pm0.03}$.

It is interesting to note that usually, anomalous heat conduction is related to the

existence of global conserved quantities [3]. This relation is not rigorous as counterexamples exist for which, despite of possessing additional global conserved quantities, the transport is *normal* [20, 21]. For our family of models, the total energy and momentum ***i.e.***, the sum over particles and scatterers, are conserved. However, we believe that our models constitute a new atypical situation in the sense that the additional global integral of motion, namely the total momentum, is not the relevant quantity for transport.

The microscopic instantaneous energy current per particle at position x^* and time t is defined as

$$j_u(x^*, t) = E(t)v(x(t), t)\delta(x^* - x(t)) \,,$$

where $E(t)$ is the energy of the particle, $x(t)$ its position and $v(t)$ its velocity. The macroscopic energy current J_U at position x^*, is thus obtained as a time average of $j_u(x^*, t)$. Thus, it follows that the relevant quantity for the J_U is the total particle momentum, which is not conserved. Whether or not our model constitutes a new type of anomalous transport, deserves further investigation.

6.1 Return to equilibrium

In order to shed more light on the anomalous heat transport we have studied the system's equilibrium response to a finite energy perturbation. Suppose that at a certain initial time, $t = 0$, the equilibrium state of the system is perturbed by an additional amount of energy ΔE that is distributed among all the degrees of freedom in a finite region of volume V, around the position x. By measuring the evolution of the energy field, one can estimate how heat propagates through the system.

Considering the closed system as in Sect. 5.1 we proceed as follows: at time $t = 0$ we perturb the state S^0 of the system to $\tilde{S}$, as follows: the energies of the particles and scatterers contained in the $\mathcal{N}$ central cells are changed so that the total energy inside these cells is E_{pert}. After this, we let the central subsystem relax. To obtain the evolution of the energy perturbation $\Delta E(x, t)$, we have followed two trajectories of the system: the unperturbed one, with initial state S^0 and the perturbed one, with initial state $\tilde{S}$. Then, the energy difference at time t and position x is

$$\Delta E(x = \lambda i, t) = \langle \tilde{E}_i(t) - E_i^0(t) \rangle \,, \tag{6.2}$$

where $\tilde{E}_i(t)$ is the energy contained in the ith cell at time t of the perturbed trajectory and respectively for $E_i^0(t)$, and $\langle \cdot \rangle$ denotes the average over an ensemble of different initial realizations.

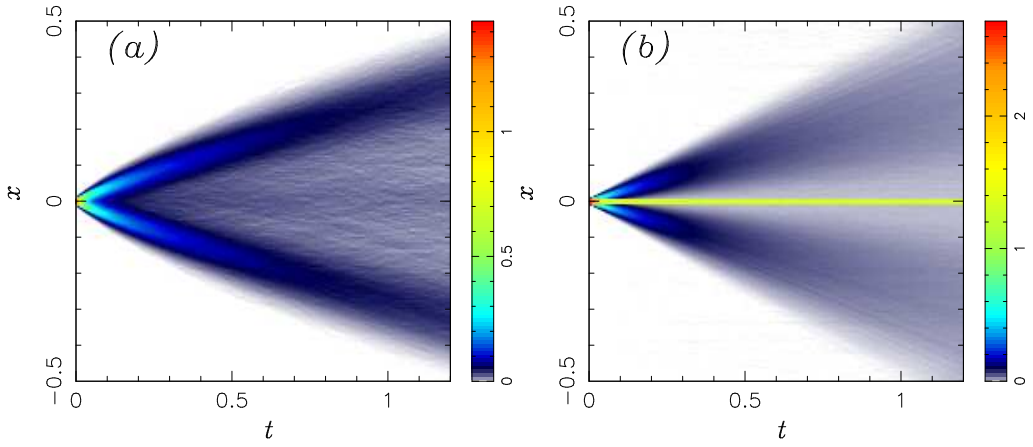

Figure 10: Evolution of the energy difference $\Delta E(x,t)$ for a chain of $N = 201$, $n = 5$ and $\sigma = 0.5$, in a quadratic color ramp. Panel (a) is for $\gamma = N$ and an initial energy per degree of freedom of $\varepsilon^0 = 5000$ and $\tilde{\varepsilon} = 50000$. Panel ($b$) is for $\gamma = 1$ and $\varepsilon^0 = 50$ and $\tilde{\varepsilon} = 500$.

When dynamical correlations are not too strong, one expects that after a sufficiently long time the perturbation $\Delta E(x,t)$ scales (with x measured from the initially perturbed cells) as

$$\Delta E(x,t) = \frac{1}{t^\xi} \Delta E \left(\frac{x}{t^\xi}, t \right) \ , \tag{6.3}$$

where the power ξ is related to the scaling of the heat conductivity with the size of the system L as [22]:

$$\kappa = N^{2-1/\xi} \ . \tag{6.4}$$

In particular, $\xi = 1/2$ corresponds to normal diffusion, while $\xi = 1$ corresponds to ballistic motion.

In Fig. 10 we show the evolution of the energy difference $\Delta E(x,t)$ for the deterministic chain $\gamma = N$ (left panel) and compare it with the stochastic chain with $\gamma = 1$ (right panel). We observe that for $\gamma = N$, the initial excess of energy at the central cell decays very rapidly. Practically none of the initial excess of energy remains in the central cell. The perturbation moves apparently ballistically,[12] to the ends of the chain, carried by two seemingly independent families of particles,

[12]The group velocity of the traveling waves depends weakly on time, probably reaching a final constant velocity at much longer times.

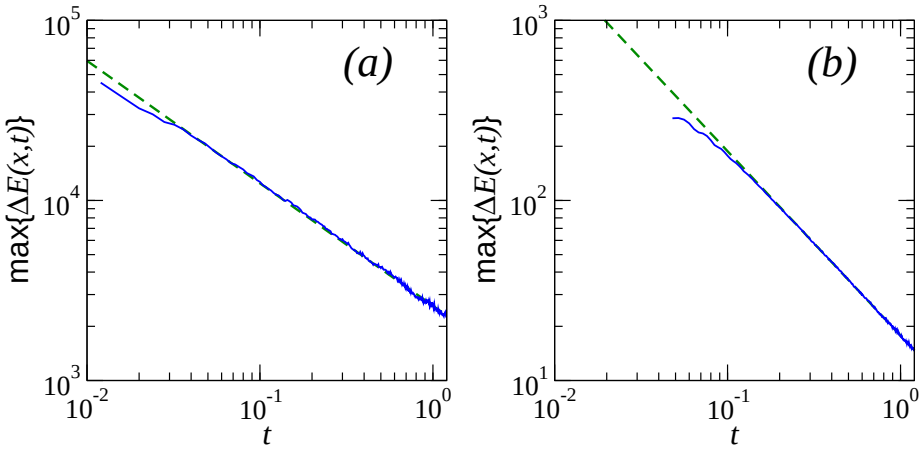

Figure 11: Damping of the maximum of the traveling waves $\Delta E(x,t)$, as a function of time (solid curves), for the same simulations of Fig. 10: $\gamma = N$ (a) and $\gamma = 1$ (b). From fits to power law (dashed lines), we obtain the scalings: (a) $\sim t^{-0.68\pm0.03}$ and (b) $\sim t^{-1.02\pm0.02}$.

those with positive velocity and those with negative velocity. The fast decay of the energy at the center that marks the existence of very strong dynamical correlations. Note for instance, that a similar observation has been made recently for a random walk with memory in the waiting times of successive steps [23]. For $\gamma = 1$, we also observe an initial fast decrease of the energy perturbation.[13] The evolution of the peaks with positive and negative velocity seems to move ballistically.

The scalings (6.3) and (6.4) are valid for the decaying of the initial perturbation, namely they are valid if measured from the decay of the central peak. Nevertheless, we find that in our system, similar scalings are possible for the traveling waves. Assuming that the excess of energy is transported across the system as a density packet, whose area is preserved on average, we show in Fig. 11 the damping of the amplitude of the moving peak as a function of time. For $\gamma = N$ (panel a), the amplitude of the peak decays approximately as $t^{-0.68}$, corresponding to a heat conductivity that scales as $\kappa \approx N^{0.53}$. On the other hand, the amplitude decay of the traveling wave for $\gamma = 1$ (panel b) is approximately t^{-1}, corresponding to a heat conductivity that grows linearly with N. To our knowledge, there is

[13]The energy excess that remains in the central cell for the whole time interval, corresponds to an excess of the scatterer energy.

no theory that addresses the scaling properties of the traveling waves that appear from the relaxation of a perturbation. However, in view of the reasonable agreement between the conductivities extracted using (6.4) and those obtained from nonequilibrium simulations, one could rephrase our findings as follows: *for the family of models that we study here, the local energy is transported by traveling waves with a local dispersion that reflects the anomalous character of the heat and particle transport.* This conclusion deserves further investigation.

Acknowledgements

We thank E. Hairer for substantial help with the programming of Eq. (2.7), and S. Lepri and F. Piazza for useful discussions. This work was partially supported by the Fonds National Suisse.

References

[1] P Collet and J-P Eckmann. A model of heat conduction. *Commun. Math. Phys.*, 287:1015–1038, 2009.

[2] F Bonetto, J L Lebowitz, and L Rey-Bellet. Fourier's law: a challenge to theorists. In *Mathematical Physics*, pages 128–150. Imp. Coll. Press, London, 2000.

[3] S Lepri, R Livi, and A Politi. Thermal conduction in classical low-dimensional lattices. *Phys. Rep.*, 377:1, 2003.

[4] A Dhar. Heat transport in low dimensional systems. *Adv. Physics*, 57:457, 2009.

[5] Z Rieder, J L Lebowitz, and E Lieb. Properties of a harmonic crystal in a stationary nonequilibrium state. *J. Math. Phys.*, 8:1073, 1967.

[6] J-P Eckmann, C A Pillet, and L Rey-Bellet. Non-equilibrium statistical mechanics of anharmonic chains coupled to two heat baths at different temperatures. *Commun. Math. Phys.*, 201:657, 1999.

[7] J Bricmont and A Kupiainen. Towards a derivation of Fourier's law for coupled anharmonic oscillators. *Commun. Math. Phys.*, 274:555, 2007.

[8] C Mejia-Monasterio, H Larralde, and F Leyvraz. Coupled normal heat and matter transport in a simple model system. *Phys. Rev. Lett.*, 86:5417, 2001.

[9] J-P Eckmann and L-S Young. Nonequilibrium energy profiles for a class of 1-d models. *Commun. Math. Phys.*, 262:237, 2006.

[10] P Grosfils, J P Boon, E G D Cohen, and L A Bunimovich. Propagation and organization in lattice random media. *J. Stat. Phys.*, 97:575–608, 1999.

[11] H Larralde, F Leyvraz, and C Mejia-Monasterio. Transport properties of a modified Lorentz gas. *J. Stat. Phys.*, 113:197, 2003.

[12] J-P Eckmann, C Mejia-Monasterio, and E Zabey. Memory effects in nonequilibrium transport for deterministic Hamiltonian systems. *J. Stat. Phys.*, 123:1339, 2006.

[13] L A Bunimovich and M A Khlabystova. One-dimensional Lorentz gas with rotating scatterers: exact solutions. *J. Stat. Phys.*, 112:1207, 2003.

[14] R Tehver, F Toigo, J Koplik, and J R Banavar. Thermal walls in computer simulations. *Phys. Rev. E*, 57:R17, 1998.

[15] P Collet and P Ferrero. Some limit ratio theorem related to a real endomorphism in case of a neutral fixed point. *Ann. Inst. Henri Poincaré*, 52:283, 1990.

[16] N Korabel and E Barkai. Pesin-type identity for intermittent dynamics with a zero Lyaponov exponent. *Phys. Rev. Lett.*, 102(5):050601, 2009.

[17] A Dhar and D Dhar. Absence of local thermal equilibrium in two models of heat conduction. *Phys. Rev. Lett.*, 82:480, 1999.

[18] G H Weiss. Some applications of persistent random walks and the telegrapher's equation. *Physica A*, 311:381, 2002.

[19] J-P Bouchaud and A Georges. Anomalous diffusion in disordered media: statistical mechanisms, models and physical applications. *Phys. Rep.*, 195:127, 1990.

[20] C Giardiná, R Livi, A Politi, and M Vassalli. Finite thermal conductivity in 1d lattices. *Phys. Rev. Lett.*, 84:2144, 2000.

[21] O V Gendelman and A V Savin. Normal heat conductivity of the one-dimensional lattice with periodic potential of nearest-neighbor interaction. *Phys. Rev. Lett.*, 84:2381, 2000.

[22] S Denisov, J Klafter, and M Urbakh. Dynamical heat channels. *Phys. Rev. Lett.*, 91:194301, 2003.

[23] V Y Zaburdaev. Random walk model with waiting times depending on the preceding jump length. *J. Stat. Phys.*, 123:871, 2006.